Polymer 51 (2010) 6021–6029

Contents lists available at ScienceDirect

Polymer

journal homepage: www.elsevier.com/locate/polymer

A biomimic shape memory polymer based self-healing particulate composite

Jones Nji [a], Guoqiang Li [a,b,*]

[a] Department of Mechanical Engineering, Louisiana State University, Baton Rouge, LA 70803, USA
[b] Department of Mechanical Engineering, Southern University, Baton Rouge, LA 70813, USA

ARTICLE INFO

Article history:
Received 21 June 2010
Received in revised form
5 October 2010
Accepted 12 October 2010
Available online 9 November 2010

Keywords:
Shape memory polymer
Self-healing
Structural damage

ABSTRACT

In a previous study, a biomimic two-step self-healing scheme (close-then-heal (CTH)) by mimicking human skin has been proposed for self-healing structural-length scale damage [Li and Uppu. *Composites Science and Technology* 2010; 70: 1419–1427]. The purpose of this study is to validate this idea by fabricating a composite with thermoplastic particles (Copolyster) dispersed in a shape memory polymer matrix (*Veriflex* Polystyrene). In this particulate composite, the confined shape recovery of the shape memory matrix is utilized for sealing (closing) cracks and the thermoplastic particles are used for molecular-length scale healing. In this study, 6% by volume of thermoplastic particles was used. Beam specimens were prepared and programmed by compression in the longitudinal direction to 6.7% of pre-strain. Structural-length scale damage was then created by producing a notch in the programmed beam specimens per ASTM D 5045. The notched beam specimens were then tested to fracture. The fractured specimens were healed per the close-then-heal mechanism and tested again to fracture. This fracture-healing test lasted for 5 cycles. The healing efficiency was evaluated per the peak-bending load. SEM was used to examine healed cracks at micro-length scale while EDS was used to evaluate molecular-length scale healing. It is found that over 65% of the peak bending load can be repeatedly recovered and the structural-length scale damage (notch) is healed at molecular-length scale.

1. Introduction

Since its introduction in the 1980s in an attempt to heal damage, restore mechanical properties and extend the service life of polymers, the concept of crack healing in polymeric materials has been widely investigated [1–15]. In thermoplastic polymers, the most widely studied and reported mechanism for self-healing is the molecular inter diffusion mechanism. It has been reported [1] that when two pieces of the same polymer are brought into contact at a temperature above its glass transition temperature (T_g), the interface gradually disappears and the mechanical strength at the polymer–polymer interface increases as the crack heals due to molecular diffusion across the interface. To better explain the process of crack healing by this mechanism, various models have been proposed [2–4,16]. In particular, Wool and O'Connor [16] suggested a five-stage model to explain the crack healing process in terms of surface rearrangement, surface approaching, wetting, diffusion and randomization. Kim and Wool [6] also presented a microscopic theory for the diffusion and randomization stages. In another study [7], it was observed that the development of the mechanical strength during the crack healing process of polymers is related to interdiffusion of the molecular chains and subsequent formation of molecular entanglements. Other reported healing mechanisms in thermoplastic polymers include photo induced healing, recombination of chain ends, self-healing via reversible bond formation, and with nanoparticles [17].

In thermoset polymers, self-healing mechanisms by the incorporation of external healing agents such as liquid healing agent (monomer) encased in hollow fibers [18,19], micro-capsules [20,21], and solid healing agent (thermoplastic particles) dispersed in the thermoset matrix [17,22], have been proposed and tested. Some polymers by themselves possess the self-healing capability such as thermally reversible cross-linked polymers [23] and ionomers [24]. Although these systems are very successful in healing micro-length scale damage, they face tremendous challenge when they are used to repair large, macroscopic, structural-length scale damage, which are visible by the naked eyes [25–27].

In order to heal structural-length scale damage, a biomimic two-step (close (first step) then heal (second step)) mechanism has been proposed by Li and Nettles [25] and detailed by Li and Uppu [26]. In this mechanism, the confined shape recovery of shape memory polymers is used for sealing or closing cracks and thermoplastic particles are used for healing at molecular-length scale. It has been

* Corresponding author. Department of Mechanical Engineering, Louisiana State University, Baton Rouge, LA 70803, USA. Tel.: +1 225 578 5302; fax: +1 225 578 5924.
E-mail address: guoli@me.lsu.edu (G. Li).

0032-3861/$ – see front matter © 2010 Elsevier Ltd. All rights reserved.
doi:10.1016/j.polymer.2010.10.021

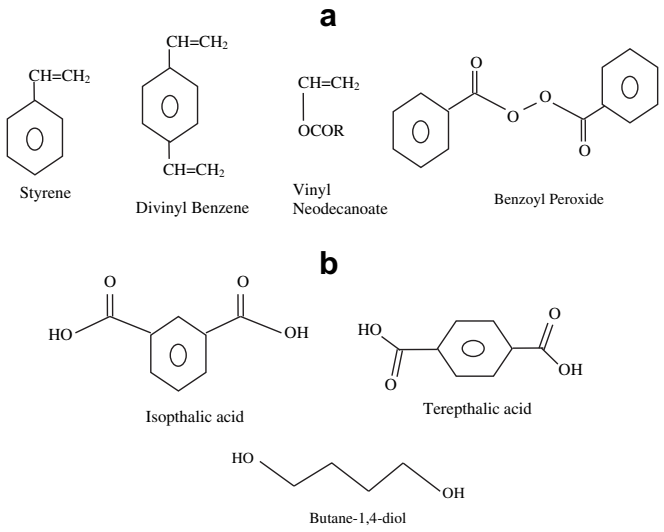

Fig. 1. Chemical structure of each component in (a) PSMP and (b) CP.

shown in previous studies that confined shape recovery (first step) can seal structural length-scale damage such as impact damage repeatedly, efficiently, timely, and almost autonomously (the only human intervention is by heating) [27–29]. As discussed by Li and Uppu in [26], the repeatability comes from the fact that each confined shape recovery leads to a new cycle of programming. It is noticed that reduction of volume during programming and external confinement during shape recovery are the key for closing internal cracks [26]. Obviously, confined compression programming can realize volume reduction. For external confinement, it has also been demonstrated that external confinement can be achieved through architectural design of structures, for instance, sandwich structures with a grid stiffened syntactic foam core [29–31] and 3-D woven fabric reinforced syntactic foam composite [27]. The second step, i.e., using thermoplastic particles for healing micro-length scale damage, has also been studied and proved [17,22]. However, the

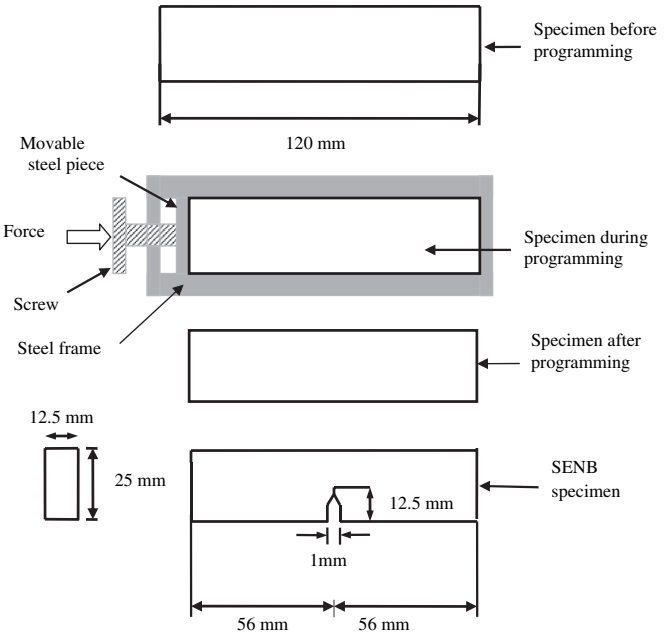

Fig. 2. Schematic explanation of the specimen preparation, programming, and notching process.

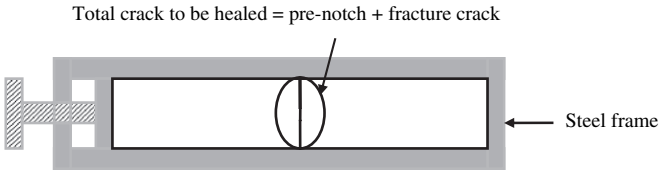

Fig. 3. Schematic of a fractured specimen in the steel frame ready for the two-step healing process.

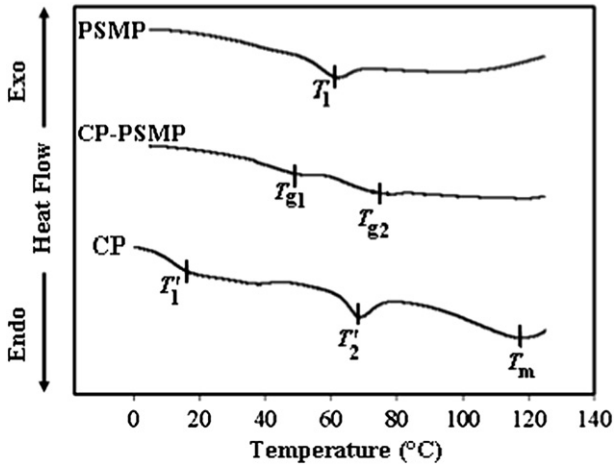

Fig. 4. Typical DSC thermograms of CP, SMP and CP-PSMP.

integration of the two steps for self-healing structural-length scale damage has not been studied experimentally.

The objective of this study was therefore to develop an SMP based particulate composite by dispersing thermoplastic particles into the SMP matrix in order to realize the CTH self-healing scheme proposed by Li and Uppu [26]. Differential scanning calorimetry (DSC) was performed in order to determine the compatibility between the thermoplastic particles and the SMP matrix. Dynamic mechanical analysis (DMA) was also performed in order to determine the glass transition temperature and viscoelastic properties of the composite. The composite was subjected to a thermo-mechanical cycle (programming, confined recovery, and free recovery) in order to determine its shape fixing and shape recovery ability. Single edge notched bend (SENB) specimens were prepared per ASTM D 5045 standard to create structural-length damage and tested in three-point bending to fracture. Healing efficiency was assessed by comparing the peak-bending load of the healed specimens to that of the original un-notched and

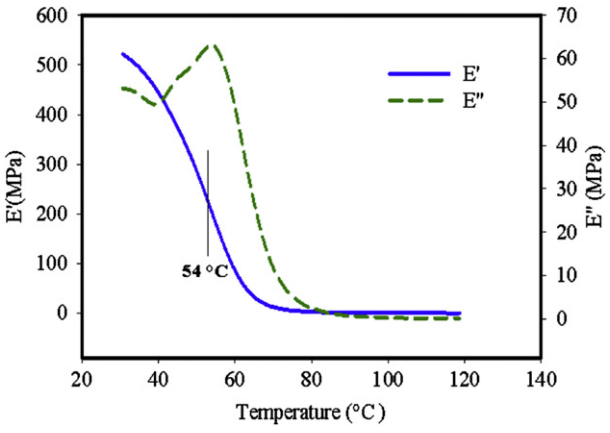

Fig. 5. Storage modulus/loss modulus–temperature plots of CP-PSMP composite.

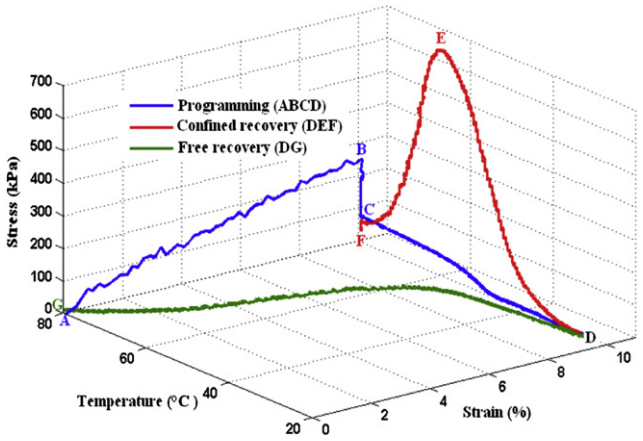

Fig. 6. A typical strain-temperature-stress plot with graphs showing the behavior of CP-PSMP during programming (ABCD), confined recovery (DEF) and free recovery (DG).

undamaged specimens. Healing efficiency was determined for up to five fracture and healing cycles. Scanning electron microscopy (SEM) was used to examine the healed cracks while energy dispersive spectroscopy (EDS) was used to understand molecular length-scale activity during the healing process.

2. Experimentation

2.1. Raw materials and fabrication method

The materials used in this study included: *Veriflex* polystyrene shape memory polymer (PSMP) from Corner Stone Research Group Inc. (glass transition temperature determined by DMA [25]: 67.71 °C, tensile strength: 23 MPa, and modulus of elasticity: 1.24 GPa at room temperature as provided by the manufacturer); and a thermoplastic polymer identified as copolyester (CP) from Abifor Inc., Switzerland (particle size: ≤ 80 μm, density: 1.3 g/cm^3, glass transition temperature determined by DSC: 17 °C and 70 °C, melting range: 114–124 °C and bonding temperature range: 125–150 °C).

The *Veriflex*® PSMP is a two-part resin system. Part A is composed of Styrene, Divinyl benzene and Vinyl neodecanoate. Part B is composed of Benzoyl peroxide. The chemical structure for each component is shown in Fig. 1 (a). The thermoplastic Copolyester is composed of Isopthalic acid, Terepthalic acid and Butane-1, 4-diol. The chemical structure for each component is shown in Fig. 1 (b).

2.2. Differential scanning calorimetry (DSC) test

Differential scanning calorimetry (TA Instruments, Q100) test was performed in order to investigate the compatibility between the PSMP and CP. The glass transition temperatures of the pure PSMP, pure CP, and their CP-PSMP composite were investigated. The sample size was 6.5 mg and the test was conducted from 0 °C to 130 °C at a ramping rate of 5 °C/min. Three effective specimens were tested to obtain an average glass transition temperature value.

2.3. Fabrication method

To produce the composite, shape memory resin was pre-heated for 2 h at 75 °C just before the thickening and curing process began. This was done in order to prevent the denser CP particles from settling to the bottom of the resin. After that, CP particles (6% by volume) were dispersed in a beaker containing the pre-heated resin. The mixture was mixed to uniformity and poured in a steel

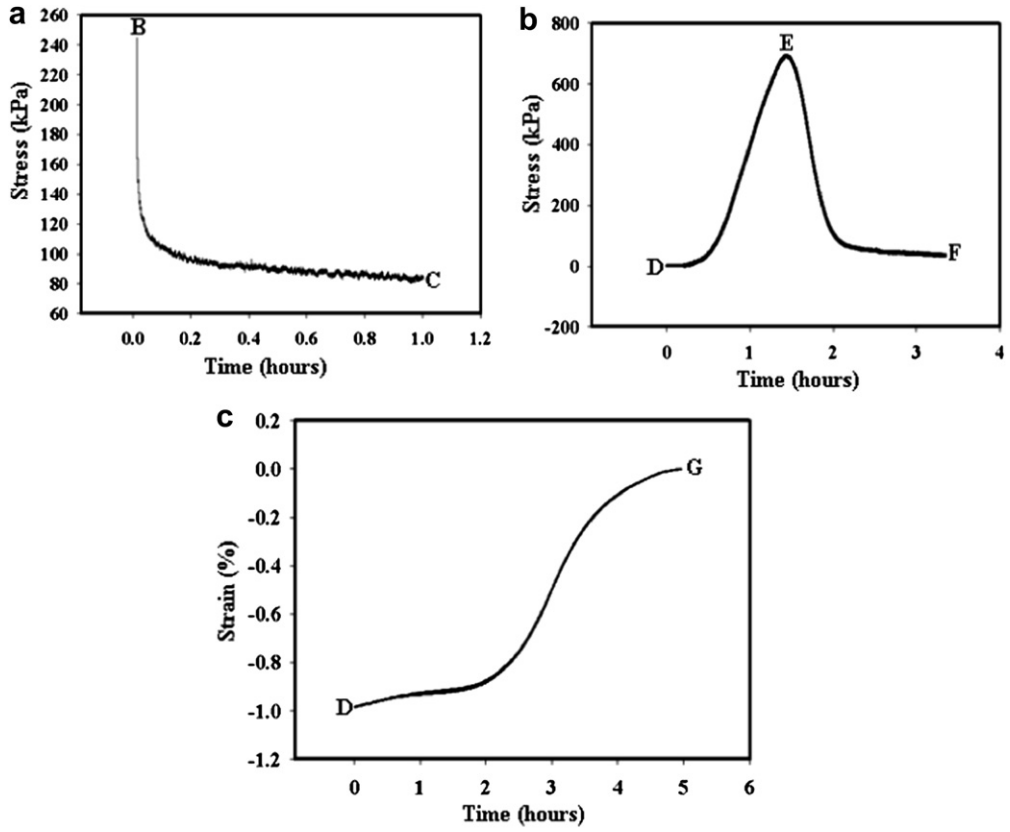

Fig. 7. Typical 2-D plots showing (a) variation of programming stress with time at 80 °C, (b) variation of confined recovery stress with time and (c) variation of free-recovery strain with time.

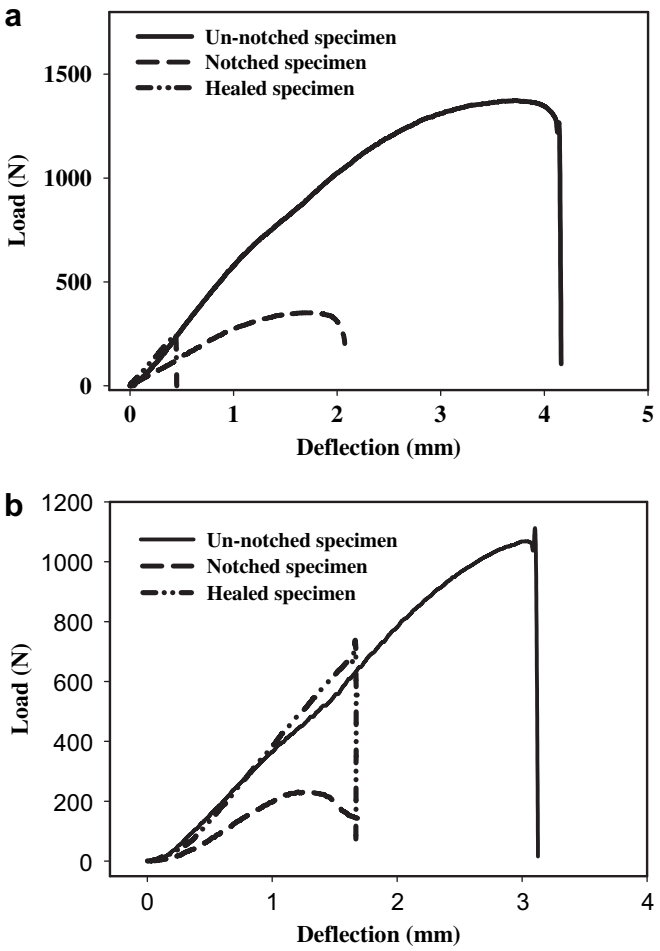

Fig. 8. Typical load-deflection curves of un-notched, notched and healed (after the first healing cycle) specimens: (a) PSMP, (b) CP-PSMP.

mold with dimensions of 300 mm × 300 mm × 12.5 mm. The mold was sealed and the material was cured in an oven as follows: 75 °C for 12 h, 90 °C for 3 h and 112 °C for 3 h. Once the curing procedure was complete, the setup was cooled down and de-molded to obtain the copolyester modified polystyrene shape memory polymer (CP-PSMP) composite.

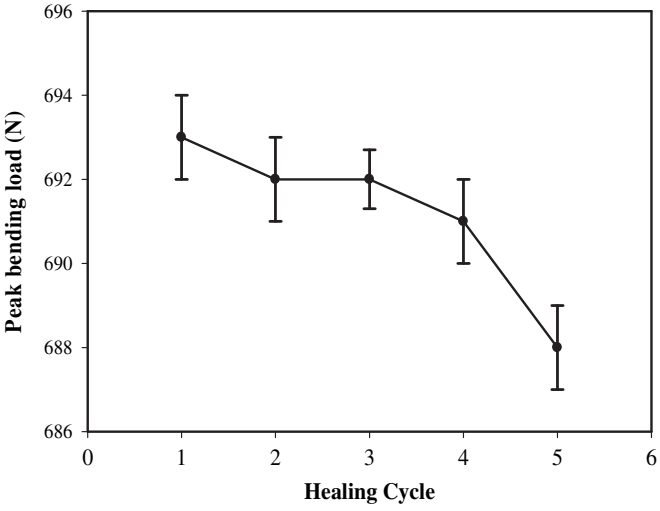

Fig. 9. Variation of peak bending load with healing cycle.

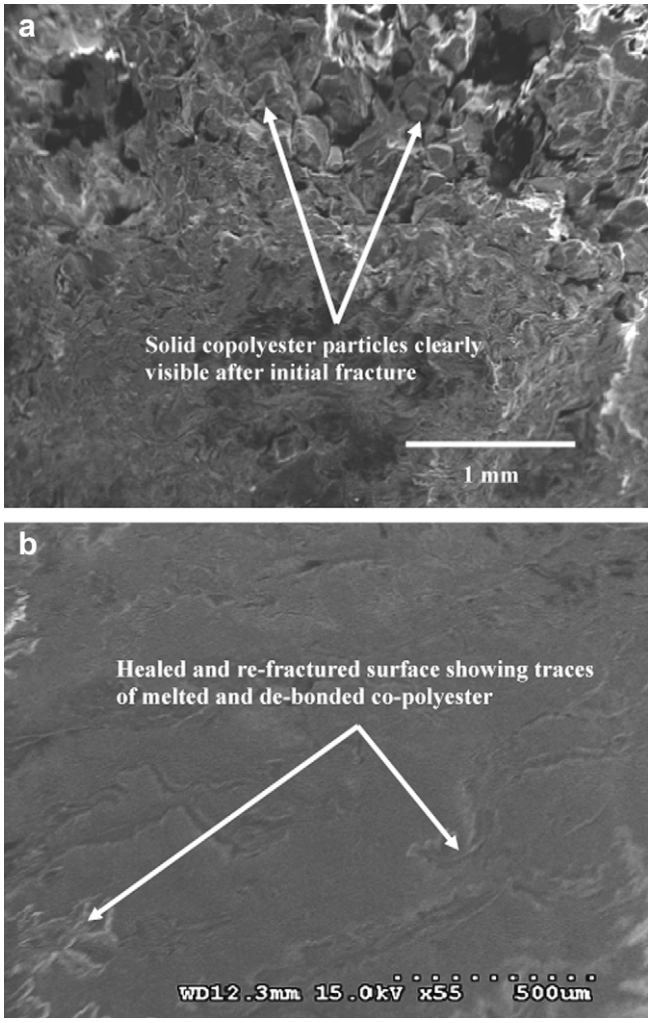

Fig. 10. SEM pictures showing fractured surfaces of a typical specimen: (a) after initial fracture, (b) after the first healing cycle.

2.4. Dynamic mechanical analysis (DMA)

Dynamic mechanical analysis was performed (Rheometic Scientific RSA III) at a frequency of 1 Hz on CP-PSMP specimens in order to determine the glass transition temperature of the composite. Rectangular tension specimens with dimensions of 36 mm × 11.5 mm × 2 mm were used. The temperature was increased at a rate of 5 °C/min.

2.5. Thermo-mechanical behavior

Compression thermo-mechanical behavior (programming and recovery) of the composite was investigated on specimens with dimensions of 25 mm × 25 mm × 12.5 mm using an MTS QTEST 150 testing machine equipped with a heating furnace (ATS heating chamber) in order to evaluate the effect of CP particles on the shape memory functionality of the CP-PSMP composite.

2.6. Beam specimen preparation, programming, and structural-length scale damage creation

Beam specimens with dimensions of 120 mm × 25 mm × 12.5 mm were fabricated by machining the cured composite slab and programmed in compression to 6.7% pre-strain in the length

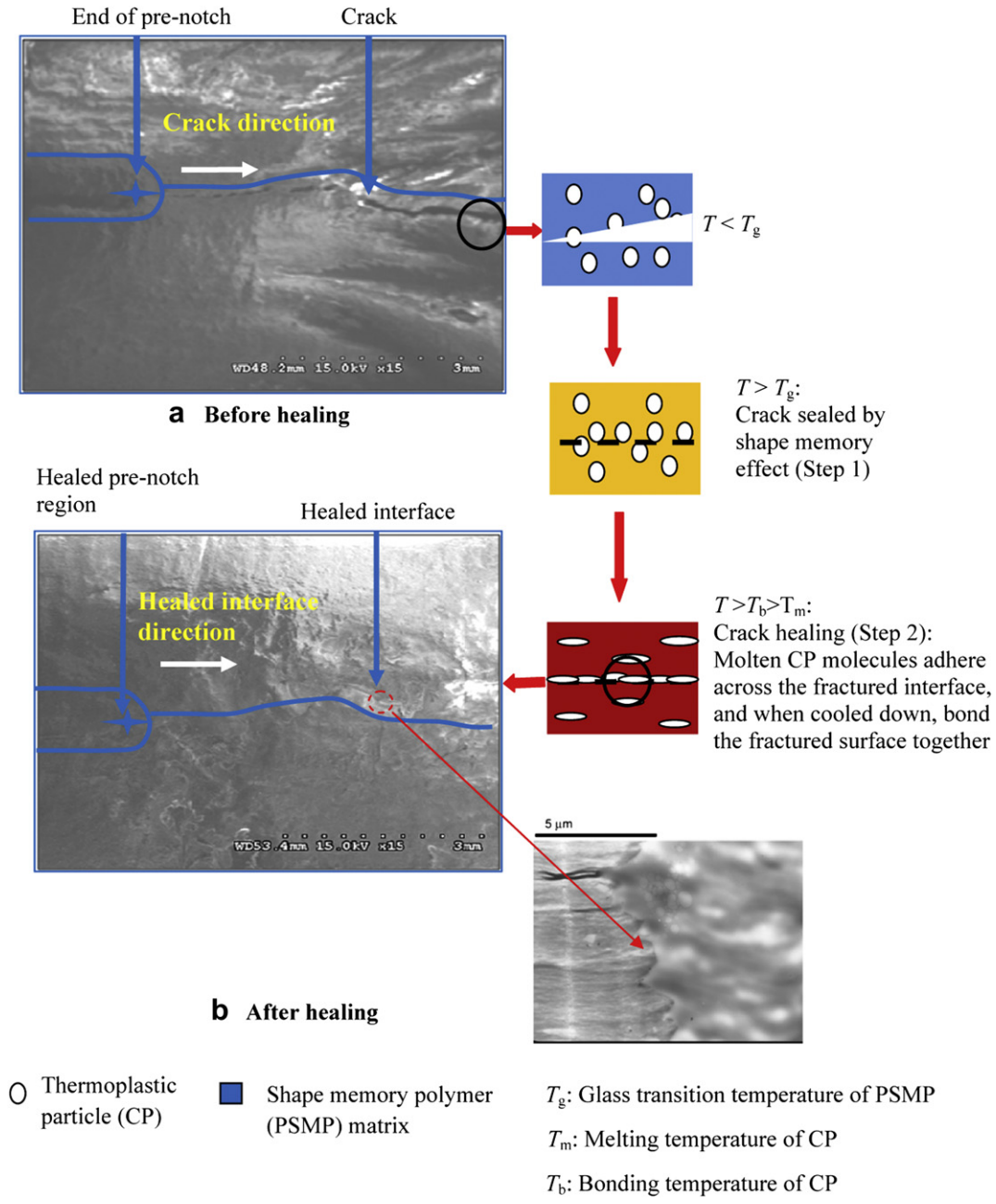

Fig. 11. Top surface view SEM pictures of a typical specimen: (a) after initial fracture and before healing, (b) after healing.

direction in an adjustable metal frame on a CARVER Model 2697 compression molding fixture. Fig. 2 is a schematic explanation of the specimen preparation, programming, and notching process. After programming, single edge notched bend (SENB) specimens were fabricated per ASTM D 5045 standard as shown in Fig. 2. The purpose of using SENB specimens was to artificially create structural-length scale damage.

2.7. Three-point bending test

Three-point bending tests were performed on a universal MTS 810 testing system with a span length of 100 mm and at a loading rate of 10 mm/min per ASTM D 5045 standard to determine the load carrying capacity of the composite using the SENB specimens. The specimens were tested and fractured completely into two halves.

2.8. Close (seal)-then-heal self-healing

Following the two-step self-healing scheme proposed by Li and Uppu [26], fractured specimens were placed in the adjustable rectangular steel frame as shown in Fig. 3 at room temperature. Once the specimen was fitted into the frame, the frame was placed on the compression-molding fixture which was pre-heated to 150 °C. It is noted that the steel frame provided confinement in the length and width directions during heating (in-plane confinement). The top surface of the framed specimen was close to the top heating plate but not in direct contact. This facilitated uniform heating of the specimen without applying confinement in the thickness direction.

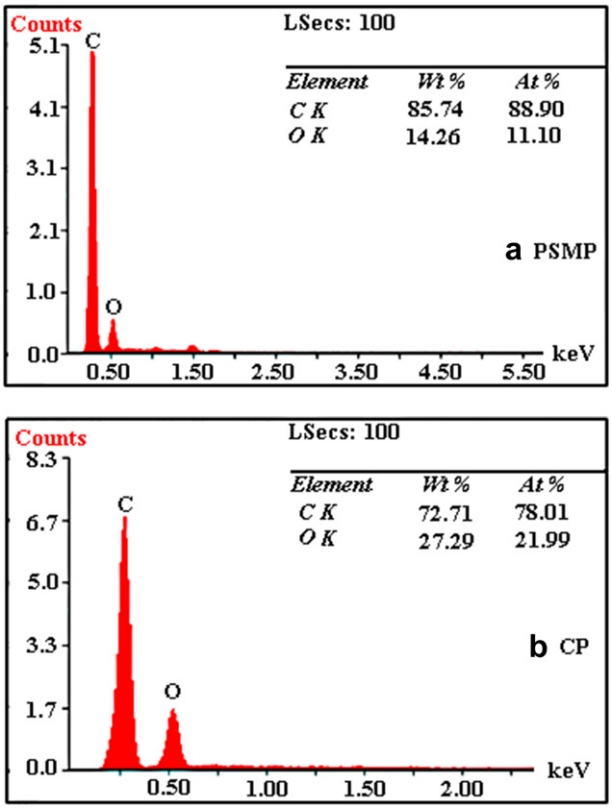

Fig. 12. EDS spectra of (a) pure PSMP and (b) pure CP.

Therefore, only 2-D in-plane confinement was used during healing. The specimens were kept within the pre-heated fixture for 20 min. During this time period, the temperature within the specimen was gradually increased; first pass its T_g, which caused shape recovery or closing of the fractured surface and the pre-notch, and then through the T_m of the CP (between 114 °C and 150 °C) causing melting of the CP, and finally to the bonding temperature of the CP (between 125 °C and 150 °C), so that the CP molecules diffused and bonded with the PSMP molecules. After 20 min, the heating plates were turned off and cooled down to room temperature. This completed the two-step self-healing scheme. Subsequent healing after fracture was done in a similar manner.

2.9. SEM observation

SEM observation was conducted (Hitachi S-3600N scanning electron microscope) in order to (1) verify that the coployester particles melted during the healing process and (2) visually verify the crack closing by examining a cracked specimen before healing and after healing.

2.10. EDS analysis

In order to verify molecular-length scale healing, energy dispersive spectroscopy (EDS, 15 kV, super ultra thin window (SUTW)-Saphire detector, AMPT: 25.6) analysis was conducted using a Hitachi 3600 N scanning electron microscope equipped with an EDAX genesis detector. The rationale was that if the CP molecules diffused into the PSMP matrix, the chemical composition near the interface will show a certain gradient. In this study, a specially prepared EDS specimen was used. To prepare the EDS specimen, a SENB specimen made of pure PSMP was fractured and a very thin layer of copolyester was placed in-between the fractured surfaces. Next, the EDS specimen was healed as described in Section 2.8. EDS analysis was conducted at and around the healed interface of the EDS specimen.

3. Results and discussion

3.1. DSC test results

In order to investigate the compatibility of the two polymers (PSMP and CP) within the composite, the single glass transition criterion [33] was adopted. Based on this criterion, PSMP and CP are compatible if the composite shows a single glass transition temperature which is in-between the glass transition temperatures of the pure PSMP and CP. Fig. 4 shows the DSC thermograms of PSMP, CP and CP-PSMP. The PSMP shows a single glass transition temperature (T_1 = 62 °C). The CP, on the other hand, shows two glass transition temperatures (T_1' = 17 °C and T_2' = 70 °C) and a melting temperature T_m (118 °C), which is within the melting range of the CP (114–124 °C provided by the manufacturer). Obviously, the CP used in this study is a copolymer as provided by the manufacturer. Between T_1 and T_1', a single glass transition temperature T_{g1} (50 °C) is observed for the CP-PSMP composite. This indicates some degree of compatibility between the PSMP and one component of the CP copolymer. The CP-PSMP composite also shows a second glass transition temperature T_{g2} = 72 °C. This should be an indication of the effect of the other component of the CP copolymer. Because the PSMP does not have the corresponding second glass transition temperature, the PSMP does not have compatibility with the second component of the CP copolymer. Therefore, it is concluded that the PSMP and CP only has partial compatibility. However, as will be shown in the DMA test results, the concentration of the second component in the CP copolymer may be very small. Therefore, the PSMP has a certain compatibility with the major component of the CP copolymer.

3.2. DMA test result

Fig. 5 shows typical storage modulus (E′)/loss modulus (E′) - temperature plots of the CP-PSMP composite. By taking the T_g as the temperature corresponding to the peak of the loss modulus, it is found that the CP-PSMP composite shows a single T_g at 54 °C. No other transition is observed above 54 °C, indicating that the component causing T_{g2} (72 °C) that was observed through the DSC test, which is an indication of the existence of the second component in the CP copolymer, may only have a small concentration. In other words, the major component of the CP copolymer has a certain compatibility with the PSMP. It is noted that the T_g (54 °C) from the DMA test is 4 °C higher than T_{g1} (50 °C) from the DSC test. This trend has been reported before in another study [25]. Based on the T_g (54 °C), the programming temperature was taken as 80 °C, which was well above the T_g.

3.3. Thermo-mechanical behavior

Fig. 6 shows a typical 3-D plot of stress, strain, and temperature for this composite (CP-PSMP) with graphs of the programming (ABCD), 1-D confined recovery (DEF) and free recovery (DG) processes. Specimens were heated to 80 °C (at point A), compressed (strain controlled mode) in the thickness direction to 10% pre-strain level (point B, loading rate: 1.3 mm/min), held at 80 °C for 1 h to stabilize the stress (point C) and cooled down to room temperature (CD). While confined in the thickness direction, the specimens were heated back to 80 °C at an average rate of 0.5 °C/min in order to determine the recovery stress of the composite (DEF). The specimens were held at 80 °C for 1 h to stabilize the stress (point F). Free-shape recovery was also

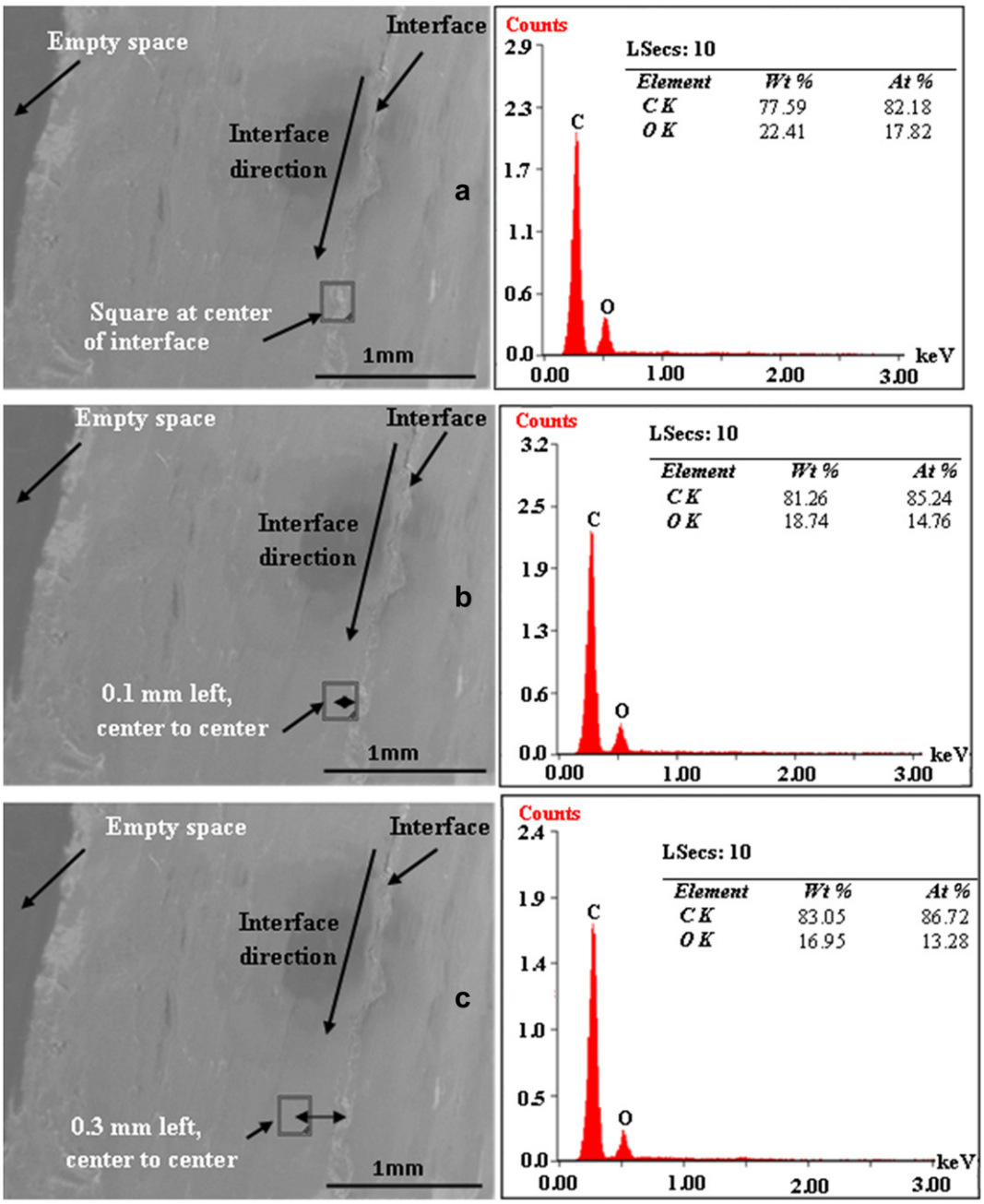

Fig. 13. Top surface view SEM pictures (left) of the EDS specimen showing a healed interface, three analysis points ((a) at the center of the interface, (b) 0.1 mm left of interface and (c) 0.3 mm left of interface) and respective EDS spectra (right).

conducted. Programmed specimens were re-heated to 80 °C (0.18 °C/min) in an oven without applying any stress to determine the free shape recovery ability of the composite by measuring displacement in the thickness direction with change in temperature (DG). A linear variable differential transducer (Cooper Instruments LDT 200 series LVDT) was used to measure the displacement while the temperature was measured and recorded with a thermocouple instrument (Yokogawa Model DC-100). The average programming stress (at point C) was found to be (74 ± 2 kPa) while the average recovery stress (point F) was (45 ± 1 kPa). The shape fixity from the programming curve was found to be 98% while the shape recovery based on the free shape recovery test was over 98%, indicating good shape memory functionality of the composite. Two-dimensional (2-D) plots showing (a) the variation of programming stress with time at 80 °C (BC), (b) the variation of confined recovery stress with time (DEF), and (c) the variation of strain with time during free recovery (DG), are presented in Fig. 7.

3.4. Three-point bending test results

Fig. 8 (a) shows typical load-deflection plots of the un-notched, notched, and healed (after the first fracture-healing cycle) pure PSMP specimens while (b) shows typical load-deflection plots of the un-notched, notched, and healed (after the first fracture-healing cycle) CP-PSMP composite specimens.

The peak loads (average of three specimens) of the originally un-notched PSMP and CP-PSMP specimens were 1385 ± 4 N and 1060 ± 3 N respectively. The maximum loads (average of three specimens) of the notched PSMP and notched CP-PSMP specimens were (358 ± 2 N) and (230 ± 2 N) respectively. This shows that the

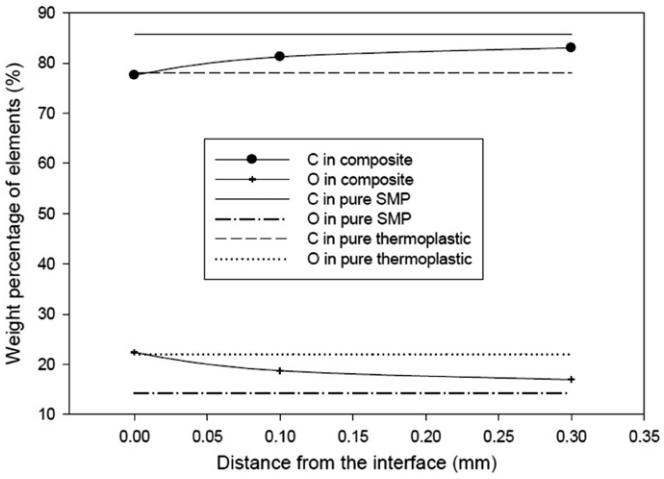

Fig. 14. Variation of component (Oxygen and Carbon) count with distance away from the healed interface.

structural-length scale damage (notch) significantly reduced the load carrying capacity of both the pure PSMP and the CP-PSMP composite. The maximum loads of the healed PSMP and CP-PSMP specimens were (250 ± 3 N) and (693 ± 3 N) respectively. Several observations can be made: (1) using crack sealing by confined shape recovery only (step 1) in the pure PSMP, the peak bending load of the resulting "healed' specimen is lower than the peak bending load of the notched specimen, indicating that the precrack (notch) and newly created crack (complete fracture of the notched beam during bending test) could not be healed by this step alone as shown in Fig. 8 (a). The reason is that the shape recovery can only narrow or close the crack, but not heal it at molecular-length scale. Therefore, under bending load, a very low healing efficiency is obtained. It is noted that in previous studies, it was found that confined shape recovery can effectively recover the lost structural capacity [28,29]. The reason is that the previous healing efficiency was evaluated in terms of compressive strength, which was not very sensitive to the existence of cracks. (2) With the two-step CTH healing, as shown in Fig. 8 (b), about 65% of the peak bending load was recovered. As compared to the notched specimen, the increase in the peak-bending load in the healed specimen is about 300%. It is believed that by changing either the concentration of the thermoplastic particles or the pre-strain level during programming, the healing efficiency could be further increased and optimized.

Fig. 9 shows typical plots of the peak bending load with fracture/healing cycle for the CP-PSMP composite. From Fig. 9, it can be seen that for five fracture/healing cycles, the proposed healing mechanism as tested through CP-PSMP specimens is reasonably repeatable.

3.5. SEM observation

Fig. 10 shows SEM pictures (fractured surface) of a typical specimen (a) after initial fracture and (b) after the first healing cycle. Solid copolyester particles are clearly visible in Fig. 10 (a). In Fig. 10 (b), solid particles are not seen but traces of melted, deformed and debonded copolyester are identified. Also, the surface in Fig. 10 (b) is smoother as compared to that in Fig. 10 (a). This is due to the compressive stress exerted on the surface during the crack sealing process (step one), resulting from the shape memory effect. This was necessary in order to keep both crack surfaces in intimate contact during the subsequent crack healing process (step two) via the melting, penetration, diffusion and bonding of copolyster across the crack interface.

Fig. 11 shows top surface view of SEM pictures of a typical specimen (a) after initial fracture and (b) after healing. In Fig. 11 (a), a crack originating from the end of the pre-notch is clearly visible. In Fig. 11 (b), the notch and the crack disappear after the two-step healing. The zoomed-in SEM picture shows good interfacial bonding.

3.6. EDS analysis

Fig. 12 shows EDS spectra of (a) pure PSMP and (b) pure CP with percentage counts of Carbon and Oxygen. The spectra were obtained to serve as baseline data. Top surface view SEM pictures showing the healed interface of the EDS specimen are presented in Fig. 13. EDS analysis was performed at three points: directly at the interface, 0.1 mm away from the center of the interface and 0.3 mm away from the center of the interface. EDS spectra corresponding to the analyzed points were recorded as shown in Figs. 13 and 14 shows the variation of Carbon and Oxygen counts in terms of weight percent with distance away from the interface. It was observed that the carbon count increased away from the interface (pure CP) while the oxygen count reduced in that same direction as the material approached pure PSMP.

From Fig. 12 (b) and 14, the oxygen and carbon counts at the interface are slightly different from the pure CP. The reason is that the counts obtained from the box immediately above the CP interlayer in the composite specimen were an average from an interaction volume, which includes the CP interlayer and may also include a small portion of the neighboring PSMP matrix. However, the interaction volume did not affect the composition in the box 0.1 mm and box 0.3 mm away from the interface. Based on Potts [32], the width of the interaction volume was about 3.4 μm. This suggests that the interaction volume for the box 0.1 mm and 0.3 mm away from the interface did not include the CP interlayer. In other words, the counts in the two boxes were due to the diffusion of the CP molecules into the PSMP matrix.

4. Conclusions

In this study, a CP-PSMP composite was developed by dispersing 6% by volume of copolyester particles in a polystyrene shape memory polymer matrix in order to realize and validate a novel biomimic two-step close-then-heal (CTH) self-healing mechanism for healing structural-length scale damage. Based on the test results, it is found that:

(1) The healing efficiency is 65% and is repeatable.
(2) The two-step scheme leads to molecular-length scale self-healing as evidenced by the EDS test results.
(3) The two-step self-healing is achieved by holding the temperature at 150 °C for 20 min. Therefore, the self-healing should be treated as timely.
(4) Because the notched specimens were fractured completely, the two-step self-healing scheme as validated by this study should be treated as being able to heal structural-length scale damage.

Further studies such as changing the volume fraction of the thermoplastic particles, changing the pre-strain levels during programming, etc., may serve to further increase the healing efficiency.

Acknowledgements

Support of this work by the National Science Foundation (NSF) (contract numbers CMMI 0946740 and CMMI 0900064) and the Louisiana Board of Regents is gratefully acknowledged and appreciated.

References

[1] Jud K, Kausch HH. Polym Bull 1979;1:697–707.
[2] Keller MW, White SR, Sottos NR. Polymer 2008;49:3136–45.
[3] Prager S, Tirrell M. J Chem Phys 1981;75:5194–8.
[4] De Gennes PG. J Chem Phys 1971;55:572–9.
[5] Doi M, Edwards SF. J Chem Soc Faradays Trans 2 1978;74:1789–801.
[6] Kim YH, Wool RP. Macromolecules 1983;16:1115–20.
[7] Kausch HH, Jud K. Rubber Process Appl 1982;2:265–8.
[8] Wool PR, O'Connor KM. Polym Eng Sci 1981;21:970–7.
[9] McGarel OJ, Wool RP. J Polym Sci Part B - Polym Phys 1987;25:2541–60.
[10] Yang F, Pitchumani R. Macromolecules 2002;35:3213–24.
[11] Chung CM, Roh YS, Cho SY, Kim JG. Chem Mater 2004;16:3982–4.
[12] Yuan YC, Rong MZ, Zhang MQ, Yang GC. Polymer 2009;50:5771–81.
[13] Takeda K, Tanahashi M, Unno H. Sci Tech Adv Mater 2003;4:435–44.
[14] Kalista SJ, Ward TC. J R Soc Interface 2007;4:405–11.
[15] Chipara M, Wooley K. Mater Res Soc Symp 2005;851:127–32.
[16] Wool RP, O'Connor KM. J Appl Phys 1981;52:5953–63.
[17] Wu DY, Meure S, Solomon D. Prog Polym Sci 2008;33:479–522.
[18] Kirkby EL, Michaud VJ, Månson JAE, Sottos NR, White SR. Polymer 2009;50:5533–8.
[19] Blaiszik BJ, Caruso MM, McIlroy DA, Moore JS, White SR, Sottos NR. Polymer 2009;50:990–7.
[20] Brown EN, White SR, Sottos NR. Compos Sci Technol 2005;65:2474–80.
[21] Brown EN, White SR, Sottos NR. J Mater Sci 2006;41:6266–73.
[22] Zako M, Takano N. J Intell Mater Syst Struct 1999;10:836–41.
[23] Chen X, Wudl F, Mal AK, Shen H, Nutt SR. Macromolecules 2003;36:1802–7.
[24] Varley RJ, Shen S, van der Zwaag S. Polymer 2010;51:679–86.
[25] Li G, Nettles D. Polymer 2010;51:755–62.
[26] Li G, Uppu N. Comp Sci Tech 2010;70:1419–27.
[27] Nji J, Li G. Smart Mater Struct 2010;19. paper No. 035007.
[28] Li G, John M. Comp Sci Tech 2008;6:3337–43.
[29] John M, Li G. Smart Mater Struct 2010;19. paper No. 075031.
[30] Li G, Muthyala VD. Comp Sci Tech 2008;68:2078–84.
[31] Li G, Chakka VS. Compos A Appl Sci Manuf 2010;41(1):177–84.
[32] Potts PJ. Hand book of silicate rock analysis. Hardcover. Springer London, Limited, ISBN 0216917948; 1987 (0-216-91794-8).
[33] Petrovic-Djakov DM, Filipovic JM, Vrhovac LjP, Velickovic JS. J Therm Anal Calorim 1993;40:741–5.